# Calaxin drives sperm chemotaxis by $Ca^{2+}$-mediated direct modulation of a dynein motor

Katsutoshi Mizuno[a,1], Kogiku Shiba[a,1], Masahiko Okai[b], Yusuke Takahashi[b], Yuji Shitaka[c], Kazuhiro Oiwa[c], Masaru Tanokura[b], and Kazuo Inaba[a,2]

[a]Shimoda Marine Research Center, University of Tsukuba, Shizuoka 415-0025, Japan; [b]Department of Applied Biological Chemistry, Graduate School of Agricultural and Life Sciences, University of Tokyo, Bunkyo-ku, Tokyo 113-8657, Japan; and [c]Advanced ICT Research Institute, National Institute of Information and Communications Technology, Kobe 651-2492, Japan

Edited by David E. Clapham, Howard Hughes Medical Institute, Children's Hospital Boston, Boston, MA, and approved October 24, 2012 (received for review October 3, 2012)

**Sperm chemotaxis occurs widely in animals and plants and plays an important role in the success of fertilization. Several studies have recently demonstrated that $Ca^{2+}$ influx through specific $Ca^{2+}$ channels is a prerequisite for sperm chemotactic movement. However, the regulator that modulates flagellar movement in response to $Ca^{2+}$ is unknown. Here we show that a neuronal calcium sensor, calaxin, directly acts on outer-arm dynein and regulates specific flagellar movement during sperm chemotaxis. Calaxin inhibition resulted in significant loss of sperm chemotactic movement, despite normal increases in intracellular calcium concentration. Using a demembranated sperm model, we demonstrate that calaxin is essential for generation and propagation of $Ca^{2+}$-induced asymmetric flagellar bending. An in vitro motility assay revealed that calaxin directly suppressed the velocity of microtubule sliding by outer-arm dynein at high $Ca^{2+}$ concentrations. This study describes the missing link between chemoattractant-mediated $Ca^{2+}$ signaling and motor-driven microtubule sliding during sperm chemotaxis.**

ascidian | Ciona | ciliary axoneme | $Ca^{2+}$-binding protein

Sperm chemotaxis toward a chemical substance released from oocytes or their associated coat is very important for the success of fertilization in many organisms, including mammals (1, 2). An increase in intracellular $Ca^{2+}$ concentration ($[Ca^{2+}]_i$) in sperm significantly alters swimming direction during chemotaxis (3, 4). Recent studies of human sperm suggest that progesterone-mediated $Ca^{2+}$ influx through a $Ca^{2+}$ channel, CatSper, plays essential role in motility changes, such as hyperactivation and chemotaxis (5, 6), although both phenomena are argued to be separated (7). However, $Ca^{2+}$ is a primary factor regulating symmetry of flagellar waveform (8, 9). Chemotactic movements are achieved by continuous changes in waveform symmetry of sperm flagella and subsequent changes in swimming direction to access the egg (10). $Ca^{2+}$-dependent regulation of flagellar beating is reportedly governed by $Ca^{2+}$-binding proteins that likely regulate axonemal dynein (8, 9). These proteins have not been identified, however, and the molecular mechanism of $Ca^{2+}$-dependent control of flagellar asymmetry in sperm chemotaxis remains uncharacterized.

Marine invertebrates are excellent models to study sperm motility because their sperm show clear motility changes and are produced in quantities sufficient for biochemical analysis. In the ascidian, *Ciona intestinalis*, a transient flagellar $[Ca^{2+}]_i$ burst is induced by a chemoattractant called sperm activating and attracting factor (SAAF), which triggers rapid sperm-turning followed by straight swimming toward eggs (4, 11). In a search for candidates that regulate $Ca^{2+}$-dependent flagellar movement, we recently identified an axonemal $Ca^{2+}$-binding protein, calaxin, which binds to outer-arm dynein in sperm flagella of *C. intestinalis* (12). Calaxin is highly conserved in metazoa, including mouse and human. In the present study, using *Ciona* sperm we show that calaxin is essential for $Ca^{2+}$-dependent modulation of sperm movement necessary for chemotaxis toward the egg. We use in vitro motility assays to demonstrate that calaxin directly suppresses microtubule sliding driven by outer-arm dynein.

## Results and Discussion

To test the function of calaxin in regulation of sperm motility in chemotaxis, we used an inhibitor of neuronal calcium sensor family proteins, repaglinide, which specifically binds to calaxin in sperm flagella (Fig. S1) (13). We first asked whether calaxin plays a critical role in sperm chemotaxis. During chemotactic movements, sperm show a unique turning movement associated with a flagellar change to an asymmetric waveform, followed by a straight-ahead movement (11). We observed sperm chemotactic movement toward a glass capillary filled with SAAF in the absence and presence of repaglinide (Fig. 1*A*). Sperm in control artificial sea water (ASW) with 0.5% (vol/vol) solvent (DMSO) showed very strong chemotaxis toward the glass capillary. However, sperm in the ASW containing 150 μM repaglinide did not exhibit the unique turn movement and showed less-effective chemotaxis (Fig. 1*A*). Linear equation chemotaxis index (LECI) (11) analysis quantitatively showed significantly decreased chemotactic property promoted by repaglinide at >100 μM (Fig. 1*B*). Sperm-swimming velocity showed no dramatic change following repaglinide treatment (Fig. 1*C*). One hypothesis is that loss of chemotactic behavior by repaglinide could be caused by an effect on $K_{ATP}$ channels (13). However, treatment with glibenclamide, a specific $K_{ATP}$ channel inhibitor, had no effect on chemotactic behavior (Fig. 1*B*). These data suggest that calaxin is essential for sperm chemotaxis.

Sperm chemotaxis is accompanied by an oscillatory $[Ca^{2+}]_i$ increase, followed by changes of flagellar asymmetry (Movie S1). To exclude the possibility that repaglinide alters chemotaxis by inhibiting oscillatory $[Ca^{2+}]_i$ increase, we compared $[Ca^{2+}]_i$ dynamics visualized by Fluo-8H during sperm chemotaxis in the absence and presence of repaglinide. Sperm treated with repaglinide showed transiently increased $[Ca^{2+}]_i$ near the chemoattractant similar to control sperm (Fig. 1*D*; Movie S2). The average maximum intensity of Fluo-8H fluorescence during chemotaxis was not affected by repaglinide (Fig. 1*E*). These results suggest that repaglinide inhibition of flagellar waveform is not due to an effect on $[Ca^{2+}]_i$, but to direct action on calaxin.

To understand how chemotaxis is inhibited by repaglinide, flagellar waveform asymmetry was analyzed in detail using a high-speed camera. In the chemotactic turn, sperm show a transient

Author contributions: K.M., K.S., M.O., Y.T., and K.I. designed research; K.M., K.S., M.O., Y.T., and K.I. performed research; Y.S. and K.O. contributed new reagents/analytic tools; K.M., K.S., M.O., Y.T., M.T., and K.I. analyzed data; and K.M. and K.I. wrote the paper.

The authors declare no conflict of interest.

This article is a PNAS Direct Submission.

[1]K.M. and K.S. contributed equally to this work.

[2]To whom correspondence should be addressed. E-mail: kinaba@kurofune.shimoda.tsukuba.ac.jp.

This article contains supporting information online at www.pnas.org/lookup/suppl/doi:10.1073/pnas.1217018109/-/DCSupplemental.

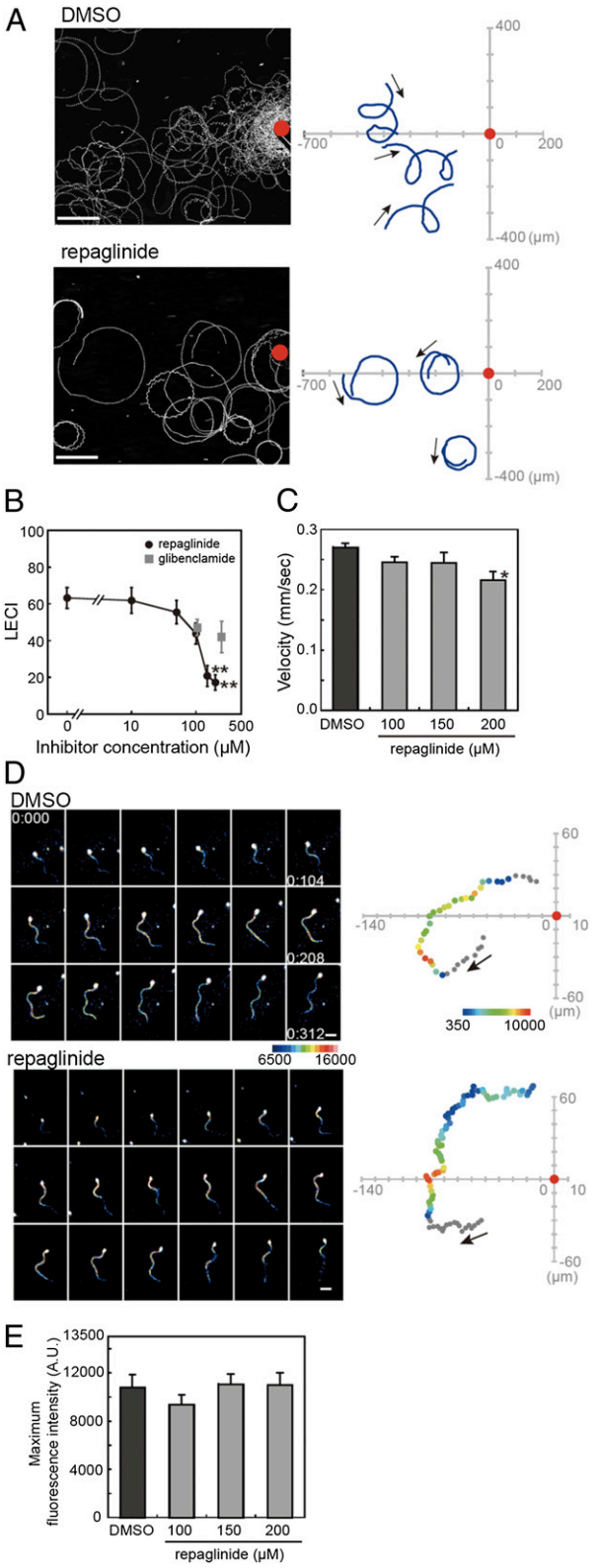


**Fig. 1.** Repaglinide inhibits sperm chemotaxis. (*A*) Sperm trajectories toward a SAAF-filled capillary (red) in the absence (*Upper*) and presence (*Lower*) of 150 μM repaglinide. (Scale bar, 100 μm.) Trajectories of three representative sperm are shown (*Right*). (*B*) Quantitation of chemotaxis using LECI. $n$ = 12–28. (*C*) Repaglinide does not significantly alter sperm swimming velocity during chemotaxis. $n$ = 30. (*D*) Pseudocolor display of $[Ca^{2+}]_i$ as sperm swim toward a chemoattractant in the absence (DMSO) or presence of 150 μM repaglinide. Sperm trajectories and the position relative to chemoattractant (red) are shown in pseudocolor display of flagellar part (*Right*). (*E*) Maximum Fluo-8H fluorescent intensity of flagellar part during chemotaxis. Repaglinide treatment does not alter the maximum $[Ca^{2+}]_i$. $n$ = 12–21. Arrows in *A* and *D* indicate direction of movement. $*P < 0.01$ vs. 0 μM; $**P < 0.001$ vs. 0 μM.

change in flagellar asymmetry (Fig. 2*A*; Movie S3). Sperm treated with 150 μM repaglinide continued to exhibit transient flagellar asymmetry, but the trajectory of movement was unstable due to incomplete turning, resulting in less-effective chemotactic movement (Movie S4). Intriguingly, repaglinide-treated sperm could not sustain an asymmetric waveform and rapidly returned to a symmetric form, in contrast to control sperm, which showed strong asymmetry during one turn (Fig. 2*A*, asterisks; Movies S3 and S4). Detailed analysis revealed that repaglinide-treated sperm showed multiple asymmetric changes during one turn (Fig. 2*B*, arrowheads; Fig. 2*C*), and the duration of the asymmetric state was decreased (Fig. 2 *B*, *Center*, and *D*). Such a decrease in duration could result in loss of a strong turn essential for chemotactic movement. The flagellar wave is composed of a large principal bend (P-bend) and a smaller reverse bend (R-bend) (9) (see Fig. S3). Asymmetry of flagellar waveform at the chemotactic turn was accompanied by both an increase of P-bend curvature and a decrease in R-bend curvature. Repaglinide-treated sperm achieved waveform asymmetry similar to that of control sperm (Fig. 2*B*, *Right*), and as a result the maximum asymmetric indices were the same as those seen in control sperm (Fig. 2*E*). Decreased duration of the asymmetric waveform and the resulting restoration of symmetric waveform led to weak orientation of sperm movement to the chemoattractant.

Next, to examine the direct effect of repaglinide on flagellar axonemes, we used a model in which sperm were demembranated with 0.04% Triton X-100 and reactivated by 1 mM ATP. Various concentrations of $Ca^{2+}$ were added to the reactivating solution, and sperm waveform was analyzed. Reactivated sperm showed $Ca^{2+}$-dependent changes in asymmetry of the flagellar waveform, as previously reported (8). Sperm flagella showed a more asymmetric waveform in solutions containing high $Ca^{2+}$ concentration (Fig. 3 *A* and *B*). Analysis of asymmetric indices at various $[Ca^{2+}]_i$ indicated that flagellar asymmetry became significant at greater than $10^{-6}$ M $Ca^{2+}$ (Fig. 3*B*). However, flagellar bending of reactivated sperm treated with 150 μM repaglinide was attenuated at high $Ca^{2+}$ concentrations, although flagellar bending propagated at low concentrations of $Ca^{2+}$ (Fig. 3*C*). Comparison of bending curvature along the flagellar length at $Ca^{2+}$ concentrations between $10^{-10}$ M (pCa10) and $10^{-5}$ M (pCa5) showed that repaglinide treatment greatly impaired bend propagation, especially at the distal portion of flagella at pCa5 (Fig. 3*C*). A similar effect was observed by specific antibody against calaxin (Fig. 3*D*). This wave attenuation occurred in both the P-bend and R-bend at pCa5 and in the P-bend at pCa10 (Fig. 3 *C* and *D*). Glibenclamide treatment had no effect on flagellar amplitude at both low and high $Ca^{2+}$ concentrations (Fig. S2). A calmodulin inhibitor W-7 slightly lowered the P-bend curvature, but it caused no significant attenuation of flagellar curvature (Fig. S2), indicating that attenuation of flagellar curvature is due to specific inhibition of calaxin, not that of CaM-like proteins in the axoneme.

Calaxin has three $Ca^{2+}$-binding motifs (EF-hand) (amino acids 62–90, 98–126, and 151–166) (12). The association of calcium with calaxin was investigated using isothermal titration calorimetry (ITC; Fig. 4*A*). The ITC data for $Ca^{2+}$ could be fitted to a three-sites sequential binding model, consistent with the motif prediction (Fig. 4*A*). Two of the three EF-hand motifs exhibited endothermic binding ($\Delta H_1$ = 8.0 kcal/mol and $K_{a1}$ = $2.3 \times 10^5$ $M^{-1}$; $\Delta H_2$ = 5.1 kcal/mol and $K_{a2} = 2.2 \times 10^5$ $M^{-1}$), and one was an exothermic site ($\Delta H_3 = -3.4$ kcal/mol and $K_{a3} = 3.5 \times$

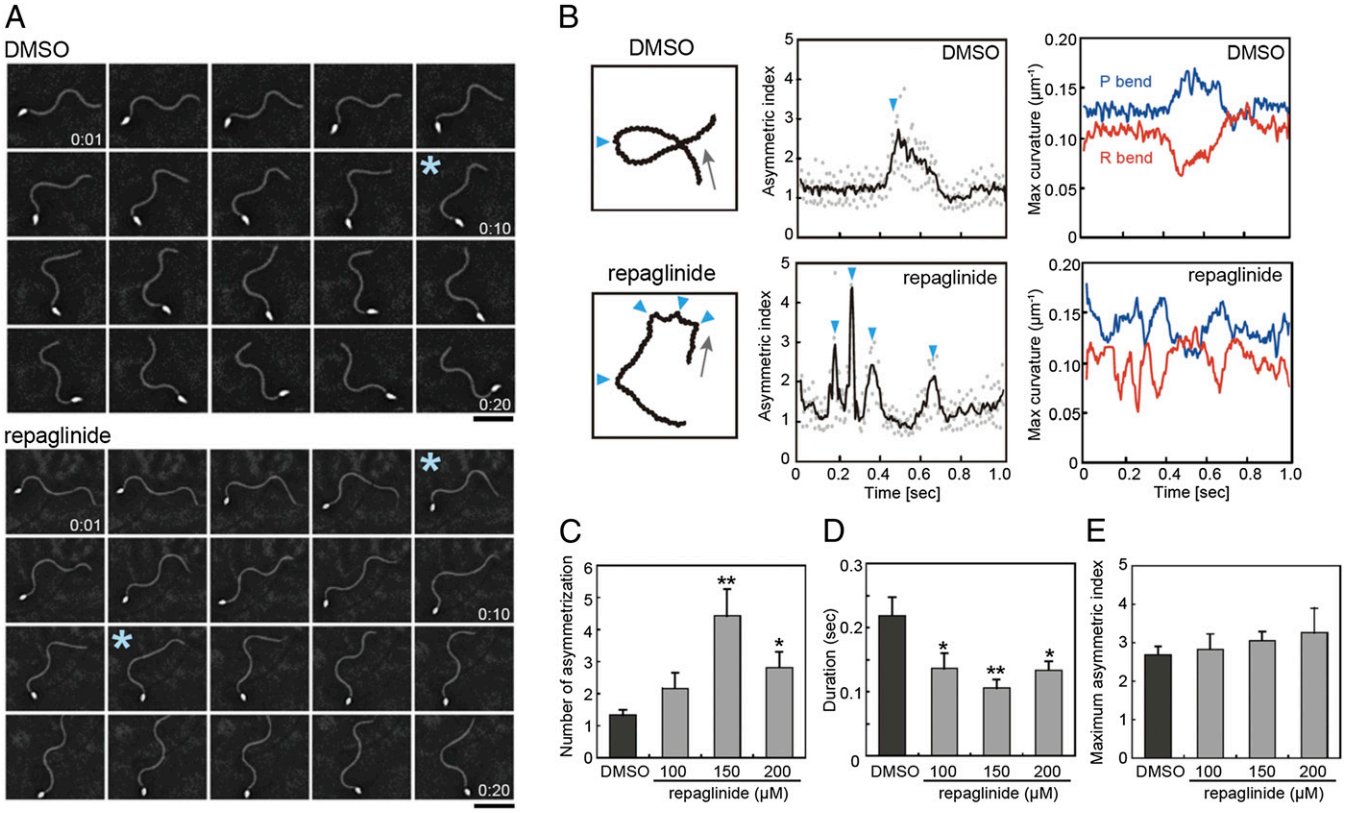


**Fig. 2.** Repaglinide treatment reduces sustainability of the asymmetric flagellar waveform at chemotactic turns. (*A*) Sequential images of sperm. Asterisks correspond to first one or two arrowheads in *B*. (*B*) (*Left*) Sperm trajectories in one turn movement. Arrows indicate direction of movement. Arrowheads indicate points of asymmetry. (*Center*) Asymmetric index. Raw data in dots are smoothed (solid line). (*Right*) Maximum flagellar curvatures of principal (blue) and reverse (red) bend during one chemotactic turn. (*C*) The number of asymmetries during one chemotactic turn is increased by repaglinide. $n = 8$–10. (*D*) Duration of one asymmetry is significantly reduced by repaglinide. $n = 12$–42. (*E*) Maximum asymmetric index during chemotaxis is not significantly altered by repaglinide. $n = 6$–10. $^*P < 0.05$ vs. 0 μM, $^{**}P < 0.01$ vs. 0 μM.

$10^4$ $M^{-1}$). Positive enthalpy reflects hydrophobic interactions, as in the cases of the $Ca^{2+}$ binding to calmodulin (14) and (+)-abscisic acid (ABA) binding to PYL1 (15).

Finally, because calaxin is a strong candidate for a direct regulator of dynein motor activity (12), we asked if calaxin modulates sliding of polymerized singlet microtubules by purified outer arm dynein in vitro. After outer arm dynein was attached to a glass slide in a chamber, microtubules were added in the presence of 1 mM ATP, and microtubule translocation was recorded (Fig. 4*B*; Movies S5, S6, S7, and S8). Outer-arm dynein from *Ciona* sperm translocated microtubules at 4.6 ± 1.5 μm/s at pCa10. Increasing the concentration of $Ca^{2+}$ to pCa5 had a small effect on translocation velocity (Fig. 4*C*). However, addition of calaxin significantly reduced the velocity of microtubule translocation at pCa5 (Fig. 4*C*). Repaglinide cancelled the suppression of microtubule translocation at pCa5 (Fig. 4*C*). A specific antibody against calaxin also cancelled the suppression effect of calaxin (Fig. 4*C*). To disrupt $Ca^{2+}$ binding of calaxin, we prepared a calaxin mutant with E118A substitution in EF-hand motif 2 (Fig. 4*A*). The E118A mutant of calaxin showed no suppression of microtubule translocation even at pCa5 (Fig. 4*C*).

Analysis of *Chlamydomonas* mutants indicates that outer-arm dyneins are essential for conversion of waveform asymmetry in response to changes in $Ca^{2+}$ concentration (16–18). Calaxin binds to the β heavy chain of outer-arm dynein (12, 19) and suppresses microtubule sliding at high $Ca^{2+}$ concentrations (Fig. 4 *B* and *C*). Such suppression is likely required to propagate the asymmetric bend. In fact, both P- and R-bends of demembranated sperm are attenuated by treatment with the calaxin inhibitor repaglinide (Fig. 3*C*) or by anti-calaxin antibody (Fig. 3*D*). During chemotaxis of repaglinide-treated sperm, the asymmetric waveform does not propagate but becomes prematurely symmetric (Fig. 2*A*). It is generally accepted that flagellar bend propagation results from alternate sliding of doublet microtubules driven by dyneins. Mechanical feedback from one bend affects microtubule sliding in an adjacent bend (20). Therefore, suppression of microtubule sliding by calaxin could affect the adjacent bend to propagate an asymmetric waveform (Fig. 4*D*).

Conversion of asymmetrical waveform in *Chlamydomonas* flagella occurs at ~$10^{-6}$ M $Ca^{2+}$ in wild-type but not in outer-armless mutants (17). ATP-sensitive microtubule binding of *Chlamydomonas* outer-arm dynein is critical between ~$10^{-6}$ M and ~$10^{-5}$ M $Ca^{2+}$ (21). Although basal level of $[Ca^{2+}]_i$ is too low (<$10^{-7}$ M) to estimate by using Fluo-8H in *Ciona* sperm, maximum asymmetric index during chemotactic turn movement (Fig. 2*E*) was comparable to that of demembranated sperm at ~$10^{-5}$ M $Ca^{2+}$ (Fig. 3*B*), suggesting that the maximum $[Ca^{2+}]_i$ during chemotactic turn is ~$10^{-5}$ M. This suggestion is compatible with the fact that $[Ca^{2+}]_i$ increases from $10^{-7}$ to $10^{-6}$ M by the chemoattractant speract in sea urchins (22). Suppression of microtubule sliding in vitro is significant at ~$10^{-5}$ M (Fig. 4*C*) and is consistent with both $Ca^{2+}$ response in sperm flagella (Fig. 3) and hydrophobic interaction formed by $Ca^{2+}$ binding to two EF-hand motifs, as suggested from ITC (Fig. 4*A*). These results further support the idea that $Ca^{2+}$-dependent suppression of microtubule-translocation activity of dynein by calaxin is a prerequisite for turn movement during sperm chemotaxis (Fig. 4*D*). Thus, $Ca^{2+}$-mediated regulation of outer-arm dynein is thought critical

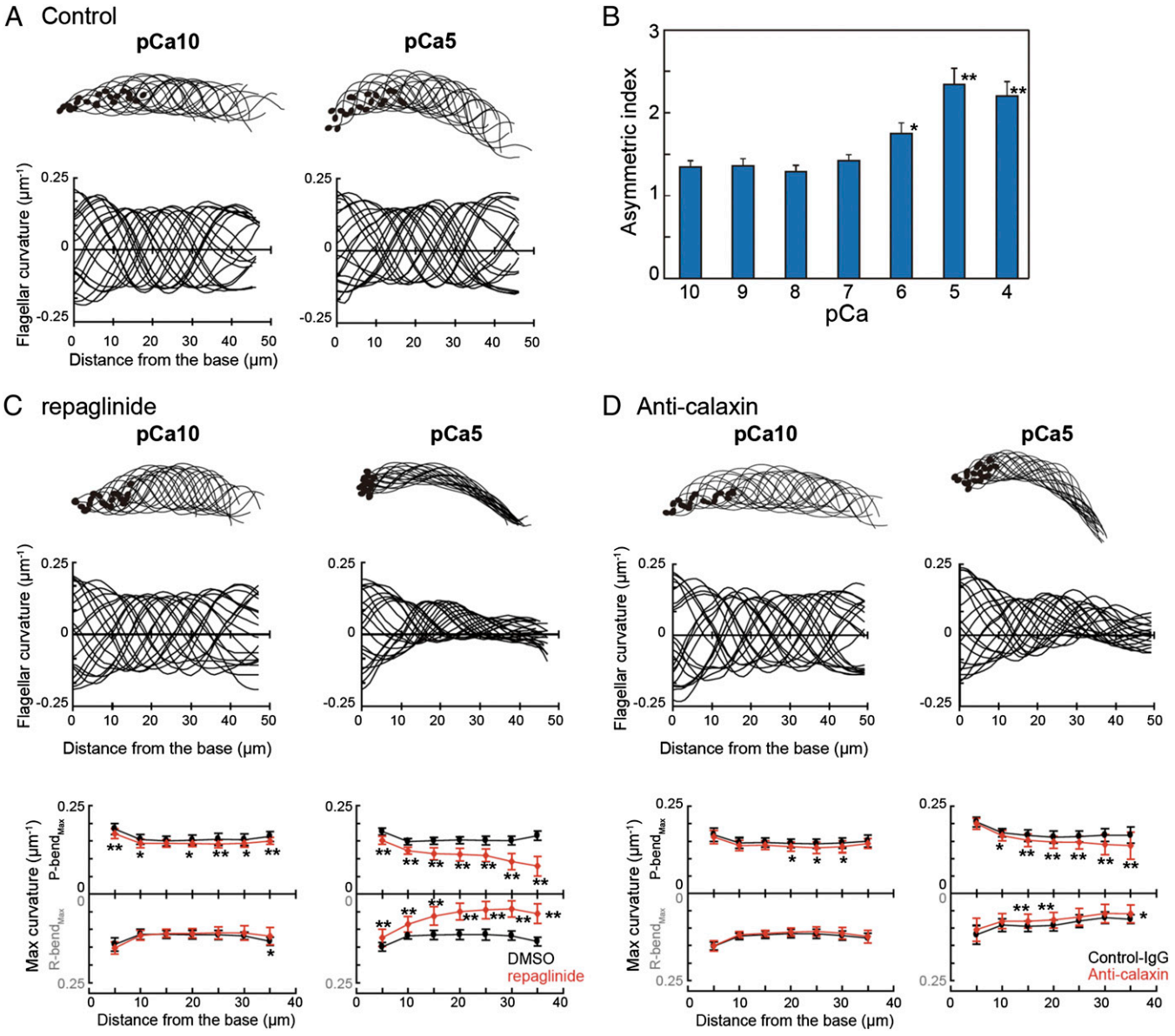


**Fig. 3.** Calaxin regulates propagation of asymmetric flagellar bending by suppressing dynein-driven microtubule sliding. (*A*) Flagellar bending pattern at pCa10 (*Left*) and pCa5 (*Right*). Twenty bending forms were chosen every 5 ms. Flagellar curvature is plotted against the distance from the base of flagellum (*Lower*). Data from 20 waveforms are overwritten. (*B*) Flagellar asymmetric indices of flagella of a demembranated sperm model were plotted at various $Ca^{2+}$ concentrations. $n = 18–19$. $^{*}P < 0.05$ vs. pCa10, $^{**}P < 0.001$ vs. pCa10. (*C* and *D*) Flagellar bending pattern and the curvature at pCa10 (*Left*) and pCa5 (*Right*) in the presence of 150 μM repaglinide (*C*) or anti-calaxin antibody (*D*). (*Bottom*) Maximum flagellar curvature against distance from the base of flagellum is plotted for P-bends and R-bends. $n = 30–40$. $^{*}P < 0.01$, $^{**}P < 0.001$.

for proper propagation of asymmetric flagellar waveform. The present study demonstrates not only the essential role of calaxin in sperm chemotaxis, but also the significance of outer-arm dynein in $Ca^{2+}$-dependent regulation of asymmetric flagellar bend. Because calaxin is commonly present in metazoan cilia and flagella (12), further studies are likely to lead to important discoveries in the $Ca^{2+}$-dependent regulation of various cilia-mediated processes.

## Materials and Methods

**Chemicals and Solutions.** Repaglinide and glibenclamide were purchased from Sigma-Aldrich, and W-7 was from Wako Pure Chemical. EAH Sepharose 4B was from GE Healthcare. Fluo-8H AM was from AAT Bioquest, Inc. Cremophor EL was from Nacalai Tesque. Other reagents were of analytical grade. The following two types of ASW were used: ASW containing 460.3 mM NaCl, 10.11 mM KCl, 9.18 mM $CaCl_2$, 35.91 mM $MgCl_2$, 17.49 mM $MgSO_4$, and 10 mM Hepes-NaOH (pH 8.2); and low-$Ca^{2+}$ ASW at pH 7 (LC7SW) containing 460 mM NaCl, 10 mM KCl, 1 mM $CaCl_2$, 36 mM $MgCl_2$, 17.5 mM $MgSO_4$, 0.1 mM EDTA, and 10 mM Hepes-NaOH (pH 7.2). LC7SW was used for loading of a fluorescent indicator. Sperm demembranation solution contained 0.2 M potassium acetate, 1 mM $MgSO_4$, 2.5 mM EGTA, 20 mM Tris·HCl (pH 8.0), 0.04% Triton X-100, and 1 mM DTT. Preincubation buffer was the same without Triton X-100. Reactivation solution contained 0.15 M $CH_3COOK$, 2 mM $MgSO_4$, 2.5 mM EGTA, 50 mM Tris·HCl (pH 8.0), 20 μM cAMP, 1 mM ATP, and 1 mM DTT. Anti-calaxin antibody was prepared according to a previous report (12). For in vitro microtubule translocation assay, IgG was purified by blot purification using GST-calaxin fusion protein.

**Repaglinide Pull-Down Assay.** The repaglinide-binding experiment was performed based on a report by Okada et al. (13). A total of 50 mg of repaglinide dissolved in 1 mL of dimethylformamide (DMF) and 100 mg of 1-ethyl-3-(3-dimethylaminopropyl)carbodiimide dissolved in 5 mL of DMF were added to the resin mixture. The pH was adjusted to 5.0, and the mixture was incubated

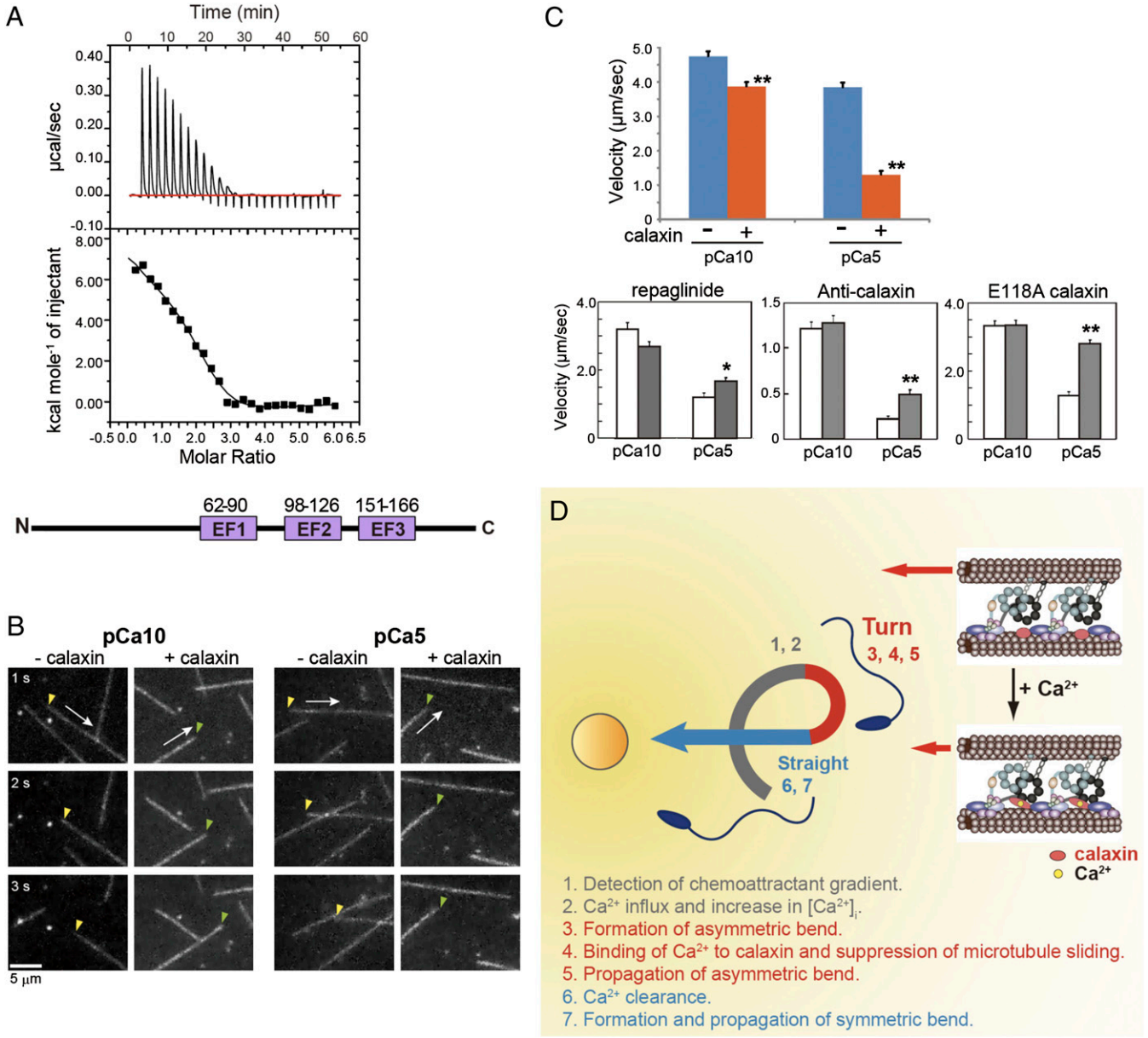


**Fig. 4.** $Ca^{2+}$ binding to calaxin suppresses dynein-driven microtubule translocation. (*A*) Isothermal titration calorimetry showing three binding sites for $Ca^{2+}$ in calaxin. (*Bottom*) Location of three EF-hand $Ca^{2+}$-binding motifs in calaxin. (*B*) Sequential dark-field images of microtubule translocation at pCa10 or pCa5 in the presence or absence of calaxin. Arrows indicate the direction of translocation. Arrowheads represent the minus (yellow) or plus (green) ends of microtubules. (*C*) Velocity of microtubule translocation. (*Upper*) Calaxin drastically suppresses translocation at pCa5. $n = 73–129$. (*Lower*) Repaglinide ($n = 40–71$), anti-calaxin antibody ($n = 107–128$), and a mutation in EF-hand 2 of calaxin ($n = 89–95$) cancel the calaxin-mediated suppression of microtubule translocation. Open bar, control; closed bar, presence of repaglinide, anti-calaxin antibody, or a calaxin mutant. $*P < 0.01$, $**P < 0.001$. (*D*) Proposed model of calaxin function in sperm chemotaxis. A chemoattractant induces $Ca^{2+}$ influx and increased $[Ca^{2+}]_i$ triggers asymmetry of the flagellar waveform. $Ca^{2+}$ binding results in a conformational change in calaxin, its association with the dynein motor domain, suppression of microtubule sliding, and propagation of an asymmetric wave necessary for turn movement.

for 24 h at 25 °C. The resin was washed once with 10 mL DMF and then three times with 10 mL distilled water, incubated with 0.2 M sodium acetate (2 mL) and acetic anhydride (1 mL) for 30 min on ice, and then incubated for 30 min at 25 °C. The resin was then washed successively with water and 0.1 M NaOH, and then equilibrated with equilibration buffer [0.15 M KCl, 20 mM Tris·HCl (pH 8.0), 1 mM $MgSO_4$ and 0.5 mM $CaCl_2$]. Sperm axonemes (0.5 mL) were suspended in 2 mL of low ion-strength buffer [1 mM Tris·HCl (pH 8.0), 1 mM EDTA] and dialyzed against ~300 mL of the same buffer for 12 h with two buffer changes. The suspension was centrifuged at 100,000 × *g* for 30 min. Extracts were mixed with repaglinide-Sepharose beads in equilibration buffer and eluted with buffer containing 0.15 M KCl, 20 mM Tris·HCl (pH 8.0), 1 mM $MgSO_4$, and 1 mM EGTA. The eluate and residual resin were separated by SDS/PAGE and immunoblotted with anti-calaxin antibody.

**Analysis of Chemotaxis.** Sperm chemotaxis was analyzed using SAAF-filled glass capillaries as described (4). Sperm movements were observed using a phase-contrast microscope (BX51; Olympus) with a 20× objective and recorded with a high-speed CCD camera (HAS-220; Ditect). A laboratory-made light-emitting diode (LED) stroboscopic illumination system was used to capture sperm flagellar waveforms. Images were taken with a frame rate of 50 frames per second (fps) or 200 fps to analyze swimming trajectory or flagellar waveform, respectively. Both properties were analyzed using Bohboh software (Bohboh Soft, Tokyo, Japan). $Ca^{2+}$-imaging analysis was performed using a Olympus filter set (excitation filter, BP490-500; dichromatic mirror, DM505; emission filter, BA510-550) and recorded on a personal computer connected to a digital CCD camera (ImagEM, C9100-13; Hamamatsu Photonics) at 50 fps using the imaging application Aquacosmos (Hamamatsu

Photonics). For fluorescence illumination, a stroboscopic lighting system with a power LED was used as described (4). Fluorescent signal intensity and sperm flagellar bending were also analyzed using Bohboh software.

**Analysis of Flagellar Waveforms.** Individual images of sperm flagella were tracked automatically, and their curvatures calculated based on the method of Baba and Mogami (23). Flagellar asymmetry was expressed as the ratio of maximal curvature of the P-bend and that of R-bend ($P\text{-bend}_{Max}/R\text{-bend}_{Max}$; Figs. S3 and S4). That ratio should equal 1 when flagella show completely symmetric bending, and greater than 1 when they show an asymmetric waveform. This ratio is referred to as the asymmetric index (4). The maximum value of the asymmetric index during chemotaxis was obtained from smoothened values of asymmetric changes to avoid overestimation.

**Motility of Demembranated Sperm.** Demembranation and reactivation of *C. intestinalis* sperm were performed using procedures based on Gibbons and Gibbons (24) and Brokaw (25) with modifications. Semen was suspended in 20 vol of $Ca^{2+}$-free ASW containing 1 mM theophylline to activate motility, and incubated for 5 min at 25 °C. Sperm were demembranated with 10 vol of demembranation solution incubated for 3 min at 25 °C. Demembranated sperm were kept for several minutes in preincubation buffer until use. Demembranated sperm were reactivated with reactivation buffer containing various $CaCl_2$ concentrations. Free $Ca^{2+}$ concentration was assessed by CALCON (18) (Table S1). Repaglinide, glibenclamide, or W-7 was added to the demembranation solution, preincubation buffer, and reactivation buffer. DMSO concentration was kept below 0.5% in all experiments. Sperm flagellar waveforms were observed as described previously. Images were recorded with a frame rate of 200 fps. Flagellar curvature and amplitude were analyzed using Bohboh software.

**In Vitro Motility Assay.** Outer-arm dynein was isolated as described (26). An in vitro motility assay was performed at 25 °C according to Sakakibara et al. (27) with modifications. All glassware was cleaned with solution containing 0.1 M HCl and 70% ethanol and rinsed with distilled water. A 10-μL flow cell was made with a glass slide and a coverslip. Porcine brain tubulin (~10 mg/mL) was polymerized into microtubules in assembly buffer [1 mM $MgCl_2$, 1 mM EGTA, 2 mM GTP, 2% (vol/vol) dimethyl sulfoxide, 80 mM Pipes/KOH (pH 6.9)] at 37 °C and then supplemented with 20 μM Taxol. Purified outer-arm dynein (250 μg/mL) was diluted in Hepes/Mg/K (HMK) buffer containing 50 mM Hepes/NaOH (pH 8.0), 4 mM $MgSO_4$, 50 mM $CH_3COOK$, 1 mM DTT supplemented with 0.5 mg/mL BSA, 2 mM EGTA, and various $CaCl_2$ concentrations (Table S2), in the presence or absence of recombinant calaxin. Final concentration of dynein or calaxin was 55 or 186 μg/mL, respectively. For testing the effect of antibody, final concentration of dynein, calaxin, or IgG was 33, 118, or 7 μg/mL, respectively. The solution was kept at room temperature for 10 min and loaded into the flow cell. After 3 min, microtubules diluted in HMK buffer supplemented with 0.5 mg/mL BSA, 0.05% methylcellulose, 1 mM ATP, 1 μM Taxol, 2 mM EGTA, and various concentrations of $CaCl_2$ were perfused into the flow cell. Microtubule gliding was observed and recorded with a dark-field optical microscope (BX51; Olympus) equipped with an immersion dark field condenser (U-DCW) and a 100-W mercury lamp (U-RFL-T). Images were recorded with a high-sensitivity camera (WAT-120N+; Watec) and captured by iMovieHD (Apple Inc.) with a video frame, and the velocity of microtubule gliding was analyzed.

**Expression and Purification of $Ca^{2+}$-Free Calaxin.** The gene of calaxin was amplified by PCR and cloned into the NdeI/BamHI site of pET-28a(+) (Novagen) to generate recombinant proteins with an N-terminal His-tag fusion. The construct of E118A calaxin mutant was generated by KOD-plus (Toyobo) and DpnI (TaKaRa). After induction of protein expression in *Escherichia coli* strain KRX, cells were harvested and proteins were solubilized in a buffer A containing 50 mM Tris·HCl (pH 8.0), 300 mM NaCl, and 10 mM imidazole. His-tag proteins were purified by Ni Sepharose 6 Fast Flow (GE Healthcare) column. Purified protein was treated with thrombin at a final concentration of 5 U/mg of His-tag fused calaxin. The solution was dialyzed against 50 mM Tris·HCl (pH 8.0), 1 mM DTT, and 1 mM EDTA at 4 °C overnight. The dialyzed solution was centrifuged at 20,000 × *g* at 4 °C for 10 min, and the supernatant was concentrated to ~1.5 mg/mL. The concentrated sample was injected onto a Superdex 75 10/300 GL column pre-equilibrated with 25 mM Tris·HCl (pH 8.0), 1 mM DTT, and 200 mM NaCl.

**Isothermal Titration Calorimetry.** ITC was carried out at 4 °C using a MicroCal $iTC_{200}$ (GE Healthcare) and a Nano ITC (TA Instruments). The protein concentration was determined by the Bradford method using BSA as the standard protein. Calaxin at 35 μM was titrated with the calcium solution [1 mM $CaCl_2$ in 25 mM Tris·HCl (pH 8.0), 1 mM DTT, and 200 mM NaCl] using 1.5-μL injections. Each injection was performed at 1,000 rpm stirring speed with injection intervals of 2 min. Curve fitting was performed using the software Origin7.

**Data Analysis.** Data were subjected to Dunnett's test for multiple comparisons or *t* tests for comparison of two independent groups. All experimental data were obtained from triplicate experiments unless indicated. The data in Fig. 3 *C* and *D* represent the mean ± SD. Other data reported in this paper represent the mean ± SEM.

**ACKNOWLEDGMENTS.** We thank H. Sakakibara, H. Kojima, and S. A. Baba for technical advice in the motility analysis. We thank all staff members of the Education and Research Center of Marine Bio-Resources, Tohoku University, and the National BioResource Project for supplying *C. intestinalis*. This work was supported in part by a grant from the Ministry of Education, Culture, Sports, Science, and Technology, Japan, and by the Japan Science and Technology Agency's Institute for Bioinformatics Research and Development (K.I.).

1. Miller RL (1985) *Biology of Fertilization*, eds Metz CB, Monroy A (Academic, New York), pp 275–337.
2. Cosson MP (1990) *Controls of Sperm Motility: Biological and Clinical Aspects*, ed Gagnon C (CRC, Boca Raton, FL), pp 104–135.
3. Guerrero A, et al. (2010) Tuning sperm chemotaxis by calcium burst timing. *Dev Biol* 344(1):52–65.
4. Shiba K, Baba SA, Inoue T, Yoshida M (2008) $Ca^{2+}$ bursts occur around a local minimal concentration of attractant and trigger sperm chemotactic response. *Proc Natl Acad Sci USA* 105(49):19312–19317.
5. Lishko PV, Botchkina IL, Kirichok Y (2011) Progesterone activates the principal $Ca^{2+}$ channel of human sperm. *Nature* 471(7338):387–391.
6. Strünker T, et al. (2011) The CatSper channel mediates progesterone-induced $Ca^{2+}$ influx in human sperm. *Nature* 471(7338):382–386.
7. Chang H, Suarez SS (2010) Rethinking the relationship between hyperactivation and chemotaxis in mammalian sperm. *Biol Reprod* 83(4):507–513.
8. Brokaw CJ (1979) Calcium-induced asymmetrical beating of triton-demembranated sea urchin sperm flagella. *J Cell Biol* 82(2):401–411.
9. Gibbons BH, Gibbons IR (1980) Calcium-induced quiescence in reactivated sea urchin sperm. *J Cell Biol* 84(1):13–27.
10. Cosson MP, Carré D, Cosson J (1984) Sperm chemotaxis in siphonophores. II. Calcium-dependent asymmetrical movement of spermatozoa induced by the attractant. *J Cell Sci* 68:163–181.
11. Yoshida M, Murata M, Inaba K, Morisawa M (2002) A chemoattractant for ascidian spermatozoa is a sulfated steroid. *Proc Natl Acad Sci USA* 99(23):14831–14836.
12. Mizuno K, et al. (2009) A novel neuronal calcium sensor family protein, calaxin, is a potential $Ca^{(2+)}$-dependent regulator for the outer arm dynein of metazoan cilia and flagella. *Biol Cell* 101(2):91–103.
13. Okada M, et al. (2003) Neuronal calcium sensor proteins are direct targets of the insulinotropic agent repaglinide. *Biochem J* 375(Pt 1):87–97.
14. Tanokura M, Yamada K (1993) A calorimetric study of $Ca^{2+}$ binding by wheat germ calmodulin. Regulatory steps driven by entropy. *J Biol Chem* 268(10):7090–7092.
15. Miyazono K, et al. (2009) Structural basis of abscisic acid signalling. *Nature* 462(7273):609–614.
16. Mitchell DR, Rosenbaum JL (1985) A motile *Chlamydomonas* flagellar mutant that lacks outer dynein arms. *J Cell Biol* 100(4):1228–1234.
17. Kamiya R, Okamoto M (1985) A mutant of *Chlamydomonas reinhardtii* that lacks the flagellar outer dynein arm but can swim. *J Cell Sci* 74:181–191.
18. Wakabayashi K, Yagi T, Kamiya R (1997) $Ca^{2+}$-dependent waveform conversion in the flagellar axoneme of *Chlamydomonas* mutants lacking the central-pair/radial spoke system. *Cell Motil Cytoskeleton* 38(1):22–28.
19. Inaba K (2007) Molecular basis of sperm flagellar axonemes: Structural and evolutionary aspects. *Ann N Y Acad Sci* 1101:506–526.
20. Morita Y, Shingyoji C (2004) Effects of imposed bending on microtubule sliding in sperm flagella. *Curr Biol* 14(23):2113–2118.
21. Sakato M, King SM (2003) Calcium regulates ATP-sensitive microtubule binding by *Chlamydomonas* outer arm dynein. *J Biol Chem* 278(44):43571–43579.
22. Wood CD, Darszon A, Whitaker M (2003) Speract induces calcium oscillations in the sperm tail. *J Cell Biol* 161(1):89–101.
23. Baba SA, Mogami Y (1985) An approach to digital image-analysis of bending shapes of eukaryotic flagella and cilia. *Cell Motil* 5(6):475–489.
24. Gibbons BH, Gibbons IR (1972) Flagellar movement and adenosine triphosphatase activity in sea urchin sperm extracted with triton X-100. *J Cell Biol* 54(1):75–97.
25. Brokaw CJ (1982) Activation and reactivation of *Ciona* spermatozoa. *Prog Clin Biol Res* 80:185–189.
26. Inaba K, Mizuno K (2009) Purification of dyneins from sperm flagella. *Methods Cell Biol* 92:49–63.
27. Sakakibara H, Kojima H, Sakai Y, Katayama E, Oiwa K (1999) Inner-arm dynein c of *Chlamydomonas* flagella is a single-headed processive motor. *Nature* 400(6744):586–590.